Design and performance of distributed helicon sources

Francis F Chen[1], John D Evans[1] and George R Tynan[2,3]

[1] Department of Electrical Engineering, University of California, Los Angeles,
56-125B Engr. IV, UCLA 159410, Los Angeles, CA 90095-1594, USA
[2] Plasma & Materials Technologies, Inc (now Trikon Technologies, Inc),
9255 Deering Avenue, Chatsworth, CA 91311-5804, USA

Abstract
Helicon plasma sources are known to be efficient generators of high-density
plasma for materials processing applications. By using multiple sources,
arbitrarily large substrates can in principle be covered uniformly with dense
plasma. To test this idea, a seven-tube helicon source was constructed, and
the plasma density and uniformity measured. Densities up to 10^{12} cm^{-3}
over a 40 cm diameter area with $\pm 3\%$ uniformity were achieved.

(Some figures in this article are in colour only in the electronic version; see `www.iop.org`)

1. Introduction

Because of their ability to produce high-density plasma
efficiently, helicon sources have been intensely studied [1, 2]
in recent years, particularly in connection with materials
processing. Helicon sources differ from other inductively
coupled radiofrequency (rf) plasmas (ICPs) in that a dc
magnetic field B_0 is required. Once the gas in the processing
chamber has been weakly ionized by the electrostatic voltages
on the antenna, the application of B_0 causes the antenna to
launch circularly polarized helicon waves; the wave energy
is subsequently converted to electron energy, thus raising the
electron temperature T_e and ionization rate. Since helicon
waves are weakly damped, the mechanism of this conversion
process is complicated [3–5] and controversial [6–8]. Our view
is that the helicon waves transfer their energy to the plasma
particles not directly but through the excitation of another
wave at the boundary. This secondary wave, a type of electron
cyclotron wave, is called a Trivelpiece–Gould (TG) mode, and
it is this wave which is readily absorbed by the plasma.

Commercial helicon reactors capable of etching 200 cm
diameter wafers have been produced [9, 10] and used [11]
successfully. A prototype source for 300 mm wafers has been
built by one of the authors (GT) and shown to give uniform
coverage. For larger substrates, a single source becomes
problematical because the energy deposition by TG modes is
computed [12] to be localized near the radial boundary, and
this would lead to a density depression near the axis. For
this reason, we have investigated the possibility of covering

[3] Present address: Department of Mechanical and Aerospace Engineering,
University of California, San Deigo, 460 EBU-II, UCSD, 9500 Gilman Drive,
La Jolla, CA 92093-0417, USA.
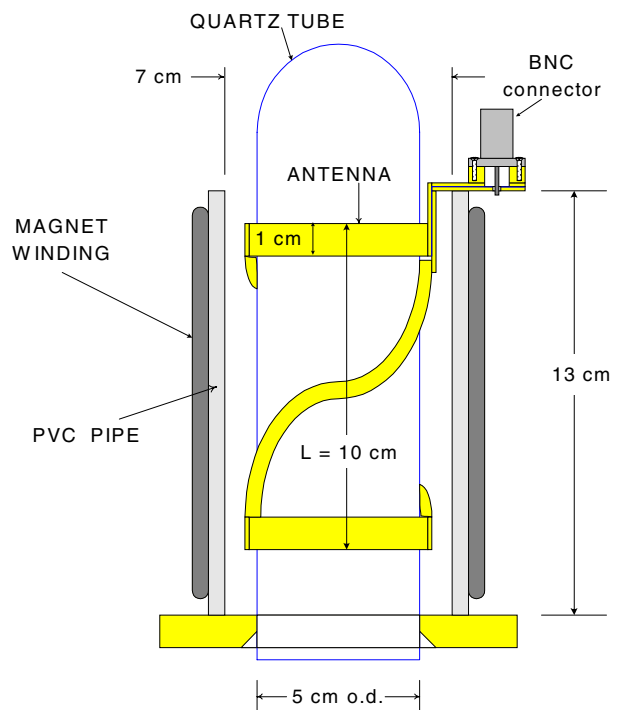
Figure 1. Schematic of a Type 1 helicon source.

large substrates with a number of small helicon sources spaced
appropriately. To prove that this is possible requires answering
the following questions: (1) What type of small source is most
suitable? (2) Can the rf power be divided equally amongst the
individual sources? and (3) Can the plasmas from each source
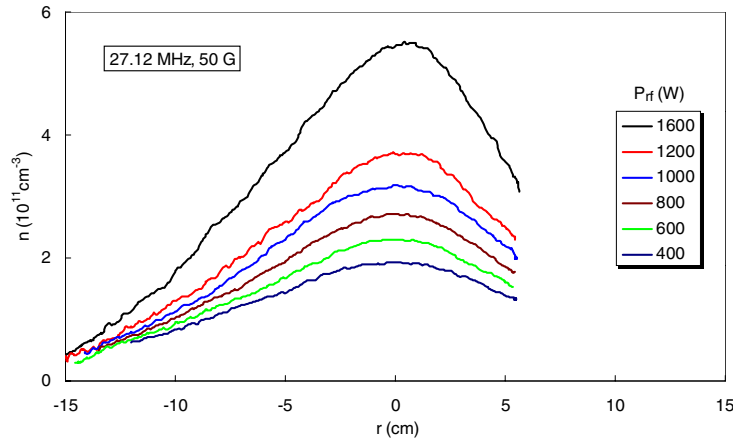
Figure 2. Radial density profiles with Type 1 source at $f = 27.12$ MHz, $B_0 = 50$ G, $p_0 = 18$ Torr of argon, and various rf powers P_{rf}, taken at $z = 6$ cm below the mounting flange and at various radii r from the axis. These definitions of f, B_0, p_0, P_{rf}, z, and r will be used in succeeding figure captions, and the gas will be argon unless otherwise noted.
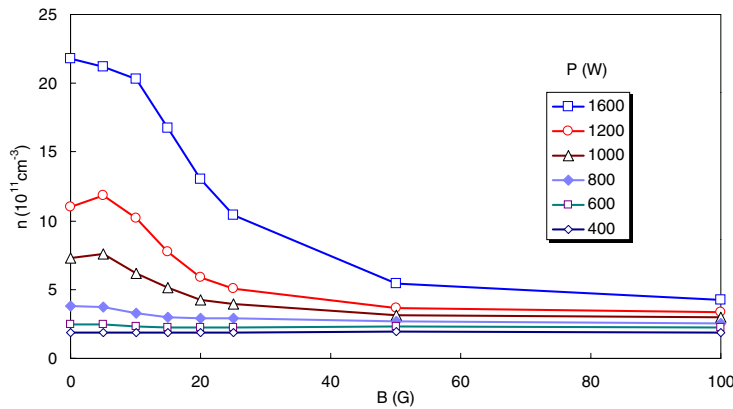
Figure 3. Peak density versus B_0 at various powers in a Type 1 source. 18 mTorr, 27.12 MHz, $z = 6$ cm, $r = 0$.
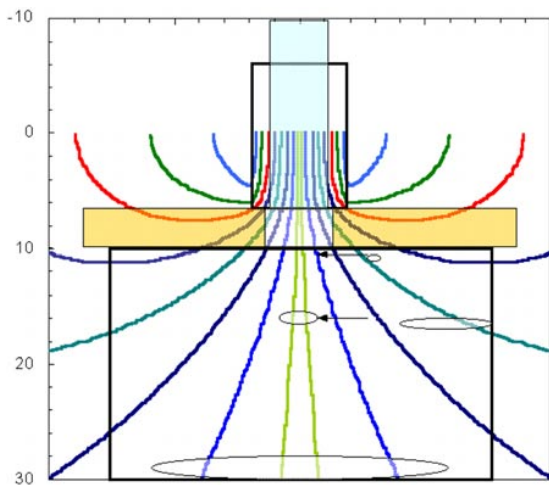
Figure 4. Schematic of the Type 1 test chamber showing magnetic field lines and outlines of the plasma tube, solenoid, entrance flange, and experimental chamber. Probe scans were made at the positions of the arrows. The ellipses show the electron Larmor orbit sizes at various positions when the field in the source B_0 is 100 G. The drawing is to scale (cm).

merge to obtain uniform, large area coverage? These questions will be answered in turn.

2. Design of individual sources

2.1. Type 1 helicon sources

Numerous experiments, confirmed by theory, have shown that the right-hand circularly polarized ($m = +1$) azimuthal mode of the helicon wave produces the highest downstream density at a given power. Our first design, the 'Type 1' source (figure 1), is therefore driven by a half-wavelength helical antenna that preferentially excites this mode [13]. A 5 cm outer diameter Pyrex tube is surrounded by a plastic coil form, on which 400 turns of 28 AWG coated magnet wire is wound to form a solenoid designed to produce a magnetic field $B_0 \leqslant 100$ G. A 10 cm long antenna is made of 1 cm wide copper sheet and fed from a matching network through a BNC connector. This design was based on a simple helicon dispersion relation [14]; for a half-wavelength antenna of length L, radius $a = 2.5$ cm, and $f_{rf} = 27.12$ MHz, this relation takes the form

$$n_{11} \approx 1.4 B_G / L_{cm} \qquad (1)$$

where n_{11} is in units of 10^{11} cm^{-3}, and B_G is the magnetic field in gauss. Thus, the 10 cm antenna is designed for $n \approx 7 \times 10^{11}$ cm^{-3} at $B_0 = 50$ G. This density is a reasonable target for the source when $n \sim 10^{11}$ cm^{-3} is desired at the
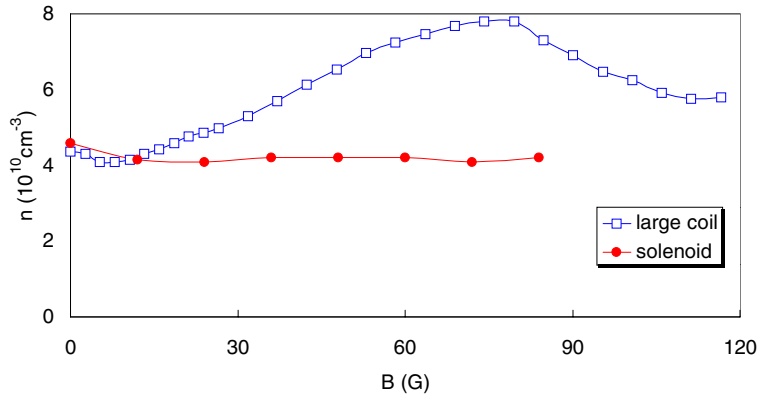
Figure 5. Comparison of Type 1 (solenoid) and Type 1A (large B_0-coil) sources. 10 mTorr Ar, 720 W, 13.56 MHz.
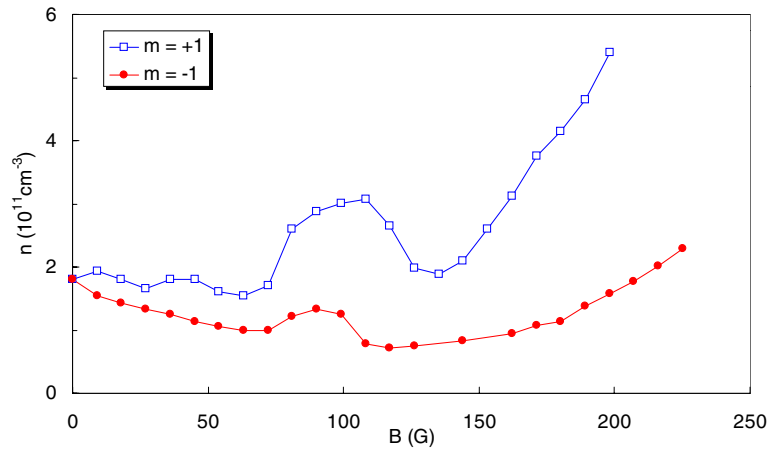
Figure 6. Low-field density peak with the Type 1A source. 10 mTorr, 1.25 kW, 13.56 MHz, $z = 3$ cm, $r = 5$ cm.
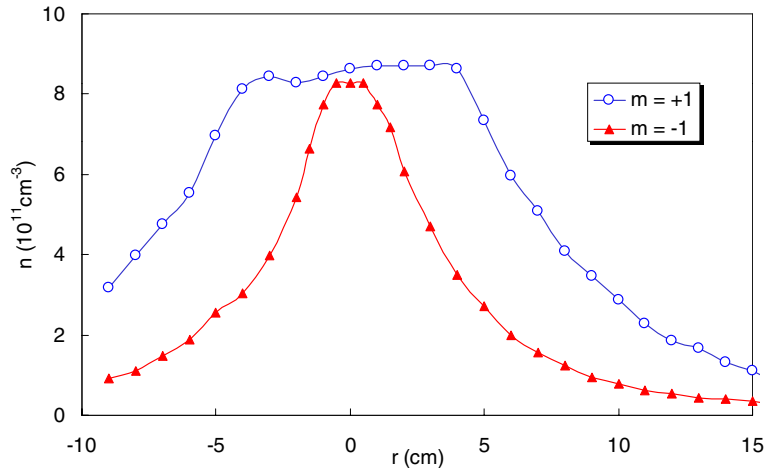
Figure 7. Density profiles of the Type 1A source centred at $r = 0$ for the $m = +1$ and -1 helicon modes. 150 G, 1 kW, 15 mTorr, 13.56 MHz, $z = 3$ cm.

substrate level. In any case, the optimum n varies with ω and B_0 over a reasonable range.

The value of B_0 was chosen to take advantage of a low-field density peak which has been observed in tubes of 4–5 cm diameter [14]. Although (1) predicts that $n \propto B_0$, this relation fails below 100 G, and a local peak in n versus B_0 is usually seen around 30–50 G. Our view [15] is that this

peak is due to an eigenmode of the combined helicon-TG wave; but whatever its cause, it offers reasonably high n at economically low B_0. Extensive measurements of the plasma injected into a processing chamber by this source have been reported earlier [16]. For instance, the $n(r)$ profile 6 cm below the flange on which the source is located is shown in figure 2 for $f = 27.12$ MHz, $B_0 = 50$ G, and various rf powers P_{rf}. These
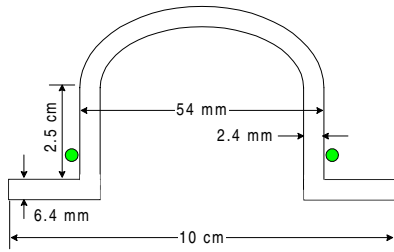
Figure 8. Schematic of a Type 2 source.

profiles indicate the coverage provided by each individual source. The width of the profile does not depend sensitively on B_0, since the field downstream is too weak to confine the plasma. Figure 3 shows the peak n for this case versus B_0. The density is seen to decrease more or less monotonically with increasing B_0, in disagreement with equation (1), and no peak occurs in the neighbourhood of 50 G, as previous uniform-field tests have shown. The reason for this behaviour, as explained in [16], is that the plasma is unmagnetized at the lowest fields and diffuses downstream unimpeded. As B_0 is increased, more and more electrons are entrained by field lines which end on the coupling flange, decreasing the number that can reach downstream. The magnetic field lines

in the single-tube chamber with a Type 1 source are shown in figure 4, along with electron Larmor orbits at various positions for $B_0 = 100$ G in the source. The Larmor radius varies from small to large relative to the scale length of ∇B_0, making numerical modelling of the source very difficult.

In spite of the difficulty with the small solenoids, the discharge inside the tube is bright blue, and $n \sim 10^{12}$ cm^{-3}, characteristic of a helicon discharge, not a weakly magnetized inductively coupled plasma. Furthermore, the discharge is much weaker when B_0 is reversed to excite the $m = -1$ mode, showing the directionality typical of $m = 1$ helicon discharges.

2.2. Type 1A helicon sources

The scrape-off problem was solved by replacing the small solenoids with a large coil of diameter comparable to that of the main chamber. A diagram of this source, 'Type 1A', can be found in [16], and the coil used is described in section 5. With this modification, the low-field density peak is readily obtained as seen in figure 5, which compares the densities for the two magnetic configurations. Figure 6 shows n versus B_0 for both directions of B_0 (corresponding to launching $m = +1$ and -1 waves downwards). For this source, both modes give comparable densities on axis, but the $m = +1$ mode produces
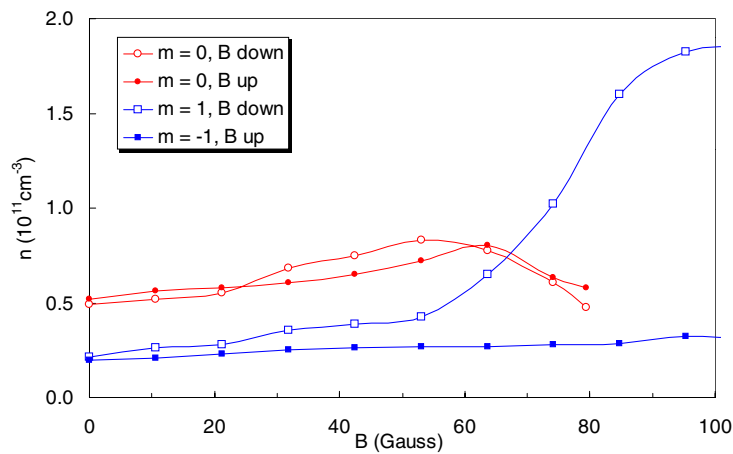
Figure 9. Density on-axis versus magnetic field with an $m = \pm1$ and a single-turn $m = 0$ antenna on a 7″ long tube, for both directions of B_0. 435 W, 10 mTorr, 13.56 MHz, $z = 3$ cm.
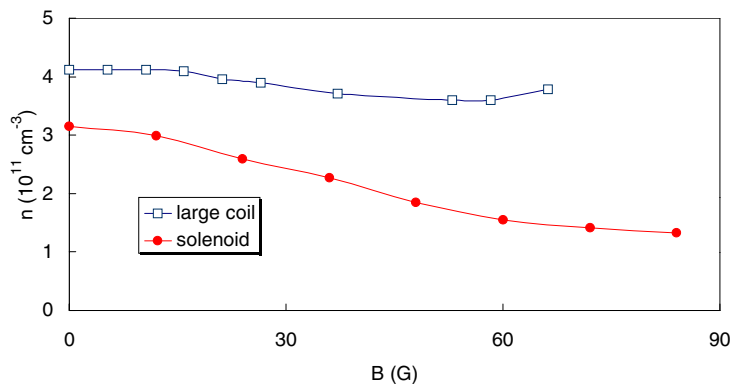
Figure 10. Density on-axis versus B_0 with an $m = 0$ antenna on a 7″ long tube, using two types of field coils. 10 mTorr, 720 W, 13.56 MHz, $z = 3$ cm, $N = 3$.
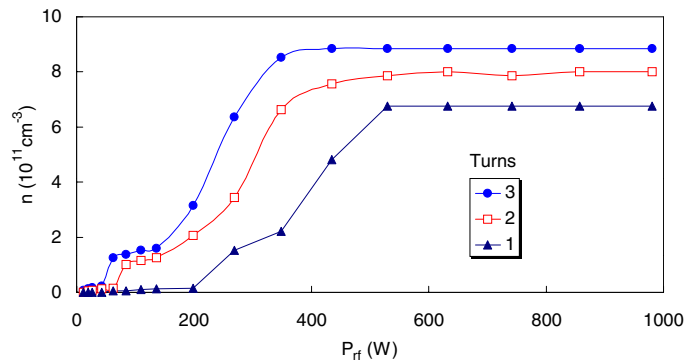
Figure 11. Dependence of n versus P_{rf} on the number of turns N in the $m = 0$ antenna. 15 mTorr, 120 G, 13.56 MHz, $z = 3$ cm, $r = 0$.
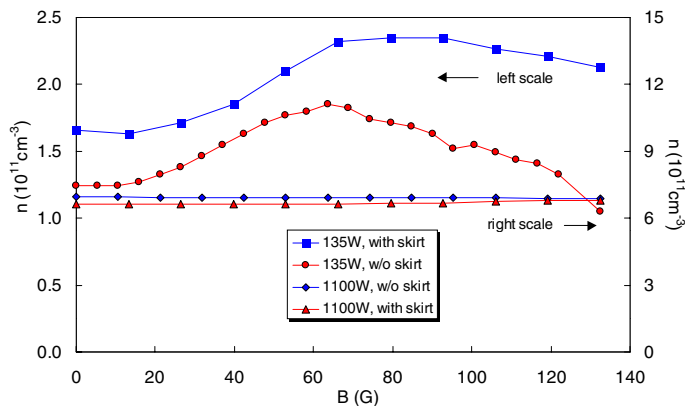
Figure 12. Effect of an insulating skirt in a Type 2 source at $P_{rf} = 135$ and 1100 W. 10 mTorr, 13.56 MHz, $N = 3$, $z = 3$ cm, $r = 0$.
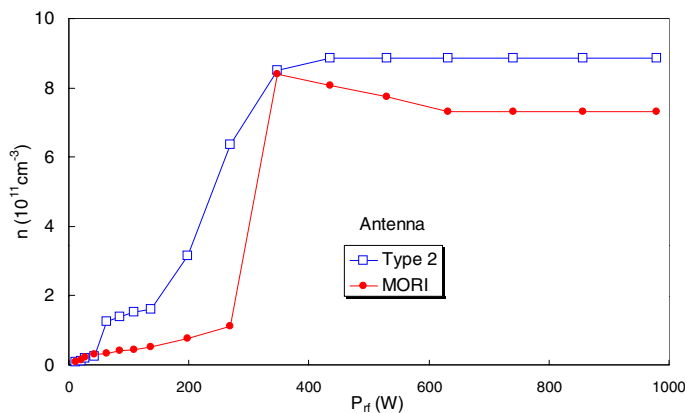
Figure 13. Density produced by a Type 2 source with $N = 3$, compared with that from a MØRI source with $L = 5$ cm ($\lambda = 10$ cm). 15 mTorr, 120 G, 13.56 MHz, $z = 3$ cm, $r = 0$.
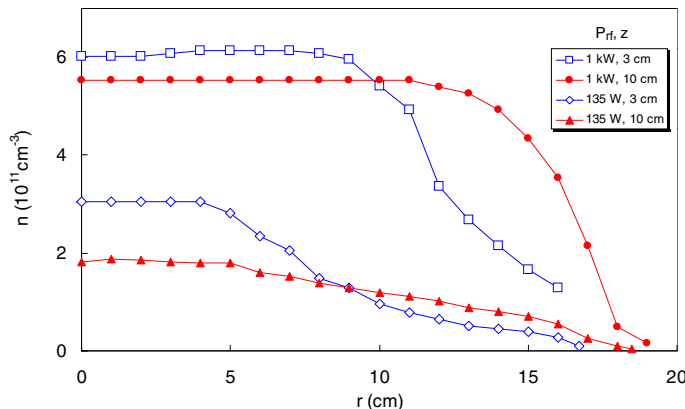
Figure 14. Density profiles illustrating the diffusion of plasma between $z = 3$ and 10 cm. 20 mTorr, 80 G, 13.56 MHz, $r = 0$.
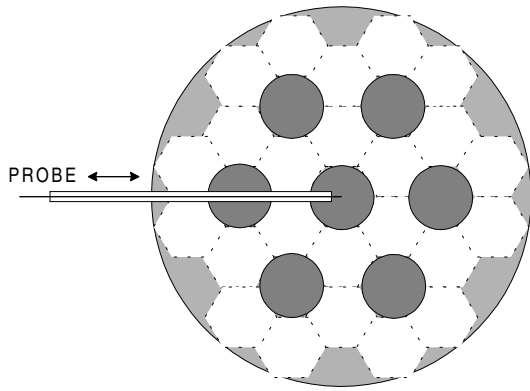
Figure 15. Arrangement of tubes in a seven-tube distributed source (conceptual diagram).

more plasma in a wider profile (figure 7), thus providing increased area coverage. Helical antennas of different lengths and with more turns, covering 1 and 2 wavelengths, were also tested, but the half-wavelength antenna of figure 1 performed the best.

2.3. Type 2 helicon sources

Research by our group [17] and others [18] shows that an $m = 0$ antenna—that is, an axisymmetric loop—is nearly as efficient as an $m = 1$ helical antenna in producing plasma, in agreement with HELIC code [19] computations. Yet another source design, 'Type 2' (figure 8) was implemented, differing from Type 1A in three primary respects. First, the antenna consists of a thin current loop, which is much more compact than a helical antenna. This loop is divided into N turns for better coupling to the rf matching network. Second, in order to prevent propagation of energy away from the chamber, the source tube is reduced to a short belljar, greatly reducing the height of the source. Finally, an insulating annulus, or 'skirt',

is added to the foot of the belljar to move the antenna from the metal flange, thus reducing parasitic losses via induced image currents. Figure 9 compares n versus B_0 for a helical ($m = \pm 1$) and a single turn loop ($m = 0$) antenna on a $7''$ long tube, for both directions ('up' and 'down') of B_0. Clearly, the $m = \pm 1$ antenna is sensitive to the sign of B_0, but the symmetric $m = 0$ antenna is not, as expected. When the inductance of the $m = 0$ antenna is optimized by varying N, both antennas produce comparable n for $B_0 < 100$ G. Figure 10 shows that the straighter field lines of a large coil give better results than a tightly fitting small solenoid in a Type 2 source, as was the case for Types 1 and 1A. As N is increased, the efficiency of the $m = 0$ antenna changes depending on the external circuitry; the optimum is $N \approx 3$–5. This variation is illustrated in figure 11. Figure 12 shows the effect of the insulating skirt. Rf powers of 135 W and 1.1 kW are shown; note that the benefit of the skirt disappears at high power.

Conventional $m = 0$ helicon sources, such as the MØRI® source [9], use two loops with current in opposite directions, spaced a half-wavelength apart ($L = \lambda/2$). However, comparison shows (figure 13) that the single-loop Type 2 source produces higher n than the MØRI source at most values of B_0. Type 2 sources also appear to have particularly good downstream properties, which can lead to large-area coverage. Figure 14 shows $n(r)$ at two axial positions, $z = 3$ and 10 cm, for $P_{rf} = 135$ W and 1 kW. The radial diffusion of plasma as it streams axially away from the source is apparent; however, at $P_{rf} = 1$ kW there is more total plasma (evaluated by integrating $n(r)$ from figure 14 over the entire cross section) at $z = 10$ cm than at $z = 3$ cm. This effect could be caused by downstream ionization, but it is not clear why it is not readily observed with the helical sources (Types 1 and 1A) as well.

3. Design of distributed sources

To avoid confusion, an individual source will henceforth be called a 'tube', including its antenna and its individual field
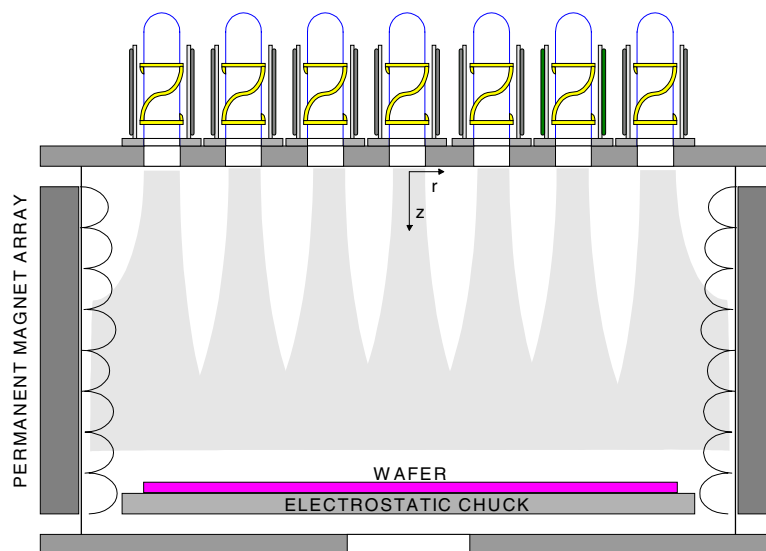
Figure 16. Schematic of a seven-tube source with a magnetic bucket. The Type 1 tubes are arranged as in figure 15 (not in line, as depicted here).
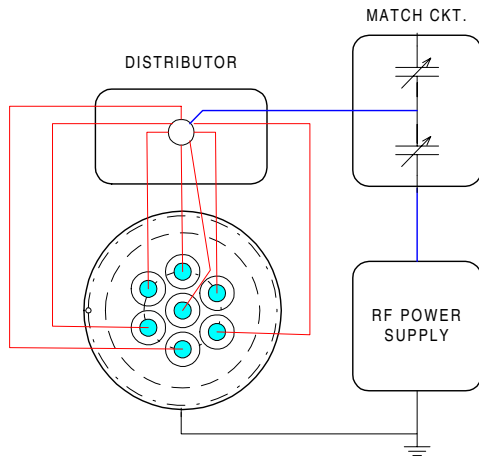
Figure 17. Schematic of the matching and distribution circuit.

coil and gas feed, if any. Power figures refer to total power to the array. The first multi-tube array consisted of seven Type 1 tubes, with one in the centre and six surrounding it; it is shown conceptually in figure 15. The source (figure 16) is placed on top of a chamber which has an array of permanent magnets on its circumference to provide confinement of primary electrons: a 'magnetic bucket'. A wafer and chuck

are shown conceptually in the figure (although not actually present in the experiment) to emphasize that they should be placed downstream in a region where the plasma is uniform, due to diffusion.

Rf power can be distributed to all the tubes from a single power supply. We have considered three ways to divide the power. First, the tubes can be connected in series. This would be necessary for plasma arcs, which have a negative resistance, so that one tube does not take all the power. Since they have a positive resistance, this is not necessary for helicon sources; in fact, a series connection has too high an impedance for a match to be obtained with reasonable values of capacitances in a conventional matching network. Second, one can consider each tube to be one element of a lumped transmission line [20]. Finally, one can simply connect the tubes in parallel [21], and this method turned out to be the best. The electrical circuit is shown in figure 17. A standard two-port capacitive matching circuit is used. Rf power is fed to seven cables of equal length (~0.5 m in most cases considered here) connecting to the individual tubes. The length of the cables must be carefully considered [22] in setting the capacitors.
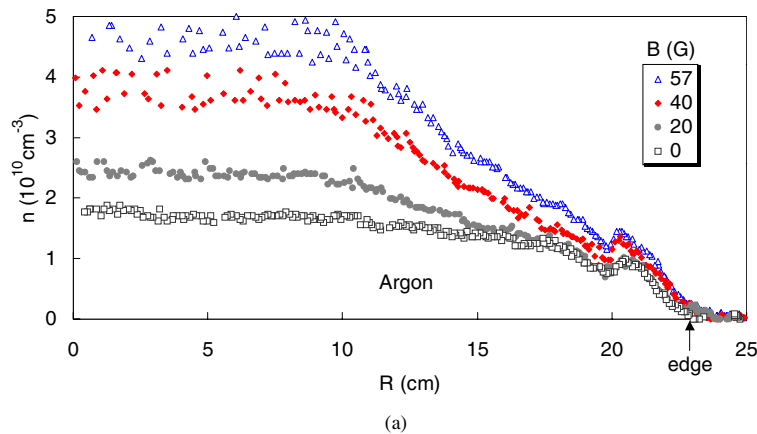
(a)
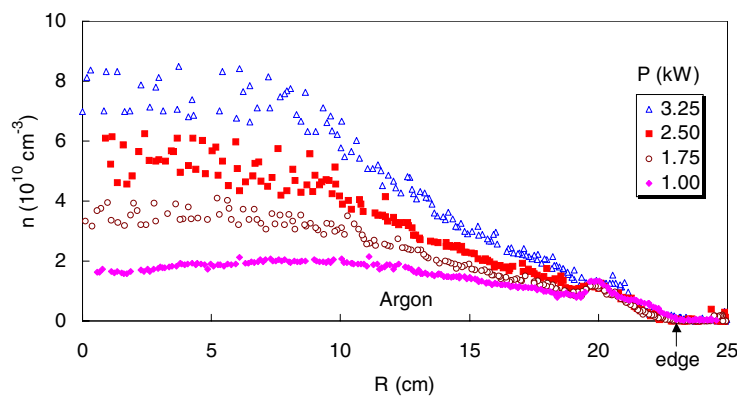
(b)

Figure 18. Density profiles along one radius of a seven-tube array of Type 1 sources versus (a) magnetic field at $P_{rf} = 1.75$ kW, and (b) rf power at $B_0 = 30$ G. 18 mTorr Ar, 13.56 MHz, $z = 9$ cm.
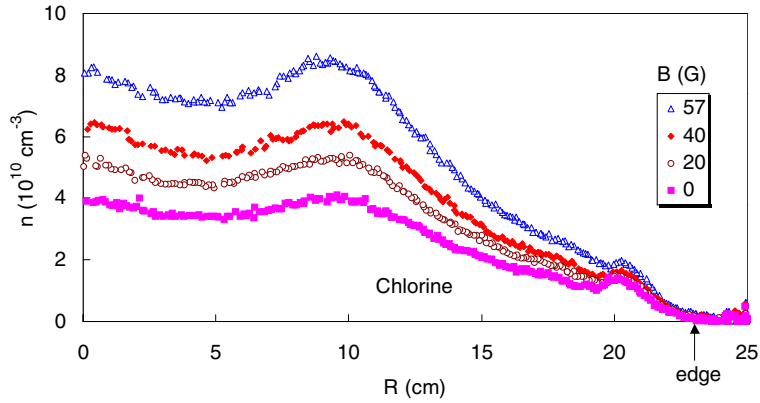
Figure 19. Density profiles along one radius of a seven-tube array of Type 1 sources versus magnetic field at $P_{rf} = 3$ kW. 10 mTorr Cl, 13.56 MHz, $z = 9$ cm.
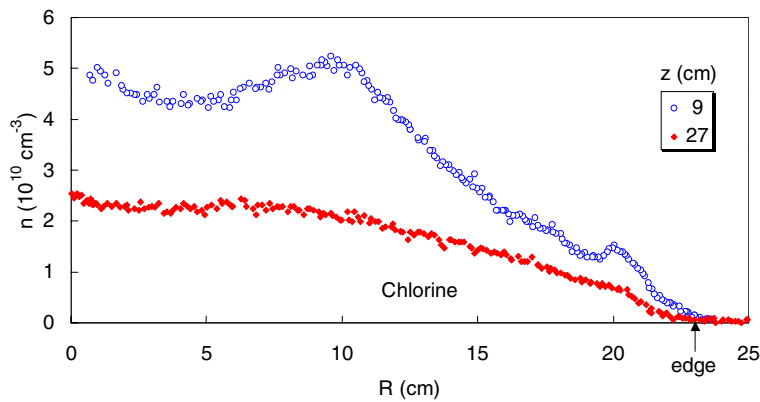
Figure 20. Diffusion of plasma in a Type 1 array source between $z = 9$ and 27 cm. 10 mTorr Cl, 2.5 kW, 13.56 MHz, 30 G.
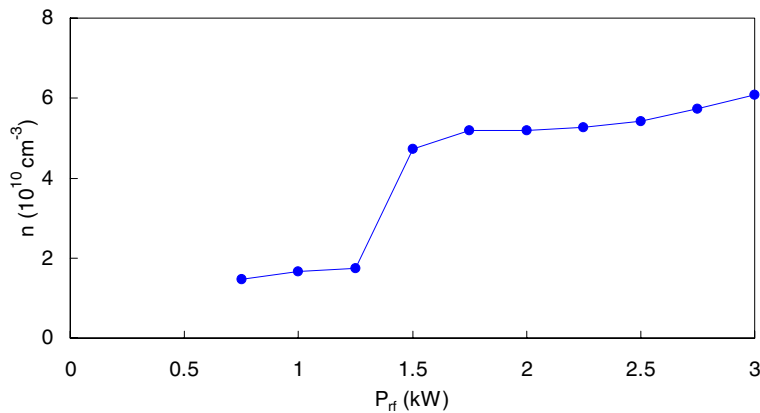
Figure 21. Jump transition in a Type 1 array as P_{rf} is increased. 10 mTorr Cl, 30 G, 13.56 MHz, $r = 0$, $z = 9$ cm.

4. Experiments with Type 1 tubes

Figure 18 shows $n(r)$ versus B_0 and P_{rf} in Ar discharges with a Type 1 '$m = 1$' array, taken with the probe shown in figure 15. Because of slower diffusion in Cl (figure 19), the structure of the individual tubes manifests itself as irregularities in the observed radial density profile. Better uniformity was observed even for Cl at $z = 27$ cm; this is shown in figure 20. Because small solenoids were used, these initial experiments produced plasma densities only in the 10^{10} cm^{-3} range and

were discontinued in favour of Type 1A and Type 2 tubes. Nonetheless, breakdown and sustainment of bright discharges in all seven tubes was achieved. The well known jump transition to the helicon wave mode is shown in figure 21 for Cl. The breakdown and sustaining powers for Ar and Cl are shown in figure 22 as functions of pressure for $B_0 = 0$. Note that once breakdown has occurred in all seven tubes, the discharge can be sustained with as little as ≈ 25 W total power. Finally, the low-field peak and directionality of a Type 1A tube array is shown in figure 23.
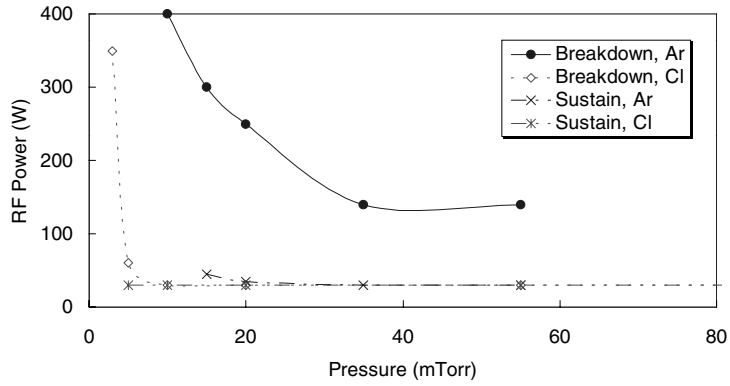
Figure 22. Rf power required to break down and sustain Ar and Cl discharges in a Type 1 array (solenoidal B_0 coils), as a function of p_0 at $B_0 = 0$.
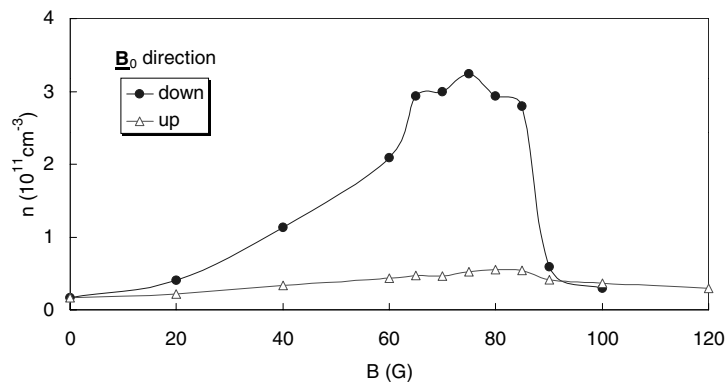
Figure 23. The low-field density peak in a Type 1A array source (large coils) is apparent when the direction of B_0 corresponds to the excitation of the $m = +1$ helicon mode. 4 mTorr Cl, 3.3 kW, 13.56 MHz, $z = 20$ cm, $r = 5$ cm.
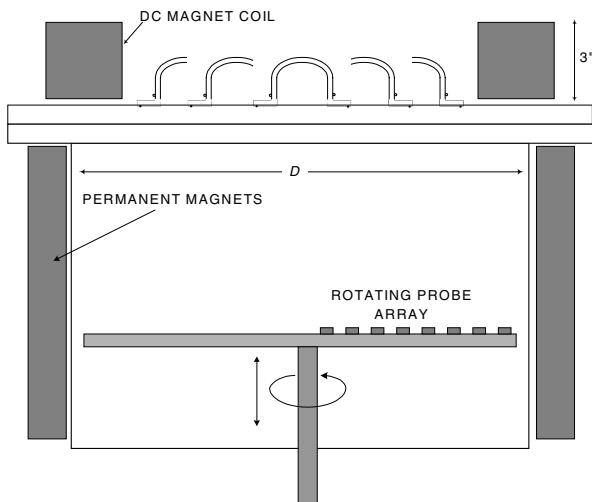
Figure 24. Schematic of a Type 2 array source with large magnet coil. Also shown is the 'Lazy Susan' rotatable ion collector array. Diameter $D = 18''$ $(14)''$ for large (small) bucket.
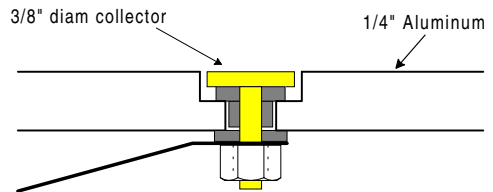
Figure 25. Schematic of an ion collector in the rotatable probe array.

5. Experiments with Type 2 tubes

For the major part of this work, an array of seven Type 2 tubes was used, encircled by a large magnetic field coil, as shown in figure 24. The tubes were arranged as in figure 15, but the diameter of the array was increased to accommodate the

larger Type 2 sources with insulating skirts. Two experimental chambers with surface-field confinement were available, with inner diameters $D = 14''$ and $18''$. Since the bolt-circle diameter of the array was designed for the smaller chamber, density profiles taken in the large chamber show a fall-off near the edge, which can easily be eliminated by adjusting the number and spatial distribution of the tubes. Also shown in figure 24 is a 'Lazy Susan' probe, consisting of eight ion collectors arranged along a radius of an aluminium plate. The plate can be moved vertically and rotated to measure azimuthal symmetry of the plasma. Figure 25 shows the design of an individual ion collector.

With a Type 2 array, densities in the 10^{11-12} cm^{-3} range were readily achieved. The insensitivity of the $m = 0$ antenna to the direction of B_0 is shown in figure 26 for a single tube and a seven-tube array. The existence of the low-field density peak in a Type 2 source is shown in figure 27. This peak appears for P_{rf} above 50 W and maximizes for $P_{rf} = 200$ W. As P_{rf} is

Figure 26. Density versus B_0 in $m = 0$ sources, showing insensitivity to field direction. $P_{rf} = 1.1$ kW, 13.56 MHz, $z = 10$ cm, $r = 5$ cm, $f = 13.56$ MHz. Top: a single tube, $N = 1$. Bottom: a seven-tube array, $N = 5$.
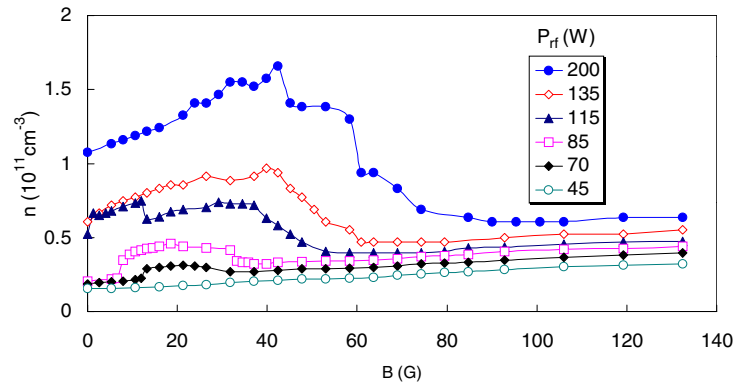
Figure 27. The low-field density peak at intermediate powers in a Type 2 array. 8 mTorr, 13.56 MHz, $N = 5$.
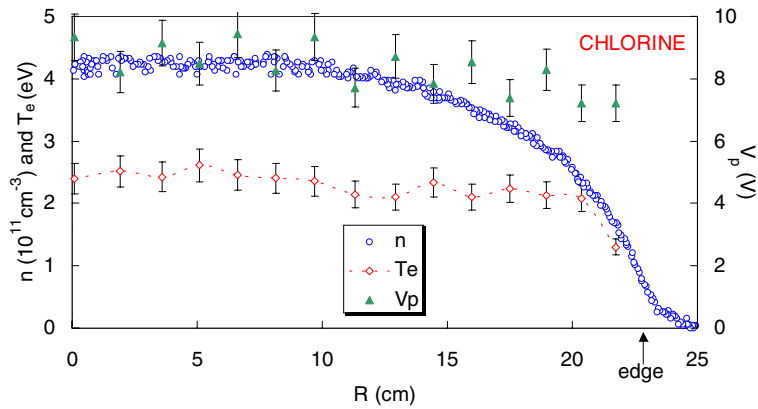
Figure 28. Radial profiles of n, T_e, and V_p in a Type 2 source. V_p is given on the right-hand scale. 3 mTorr Cl, 35 G, 3 kW, 13.56 MHz, $z = 27$ cm.

raised to greater than 300 W, the density keeps rising and does not fall at high fields. The downstream plasma conditions are shown in figure 28 for Cl. The density is uniform but falls off radially for the reason given above. The electron temperature is constant at ≈ 2 eV, and the plasma potential V_p is nearly constant at ≈ 8 V.

Density profiles near the source are given in figure 29 for argon and figure 30 for chlorine as functions of (a) B_0 and (b) P_{rf}. Note that densities approaching 2×10^{12} cm^{-3} over a 30 cm diameter are achieved in argon. Ignition in chlorine is more difficult, and some of the tubes did not fire under some

conditions. Figure 31 shows more uniform density profiles 27 cm downstream, where n is still $\sim 10^{12}$ cm^{-3} in argon.

To prove the principle of distributed sources, it is important to show that the plasma from the individual tubes diffuses fast enough to give a uniform density profile within a reasonable distance of the source. For this reason, the Lazy Susan probe was developed to measure the azimuthal symmetry of the ion flux at wafer level. Saturation ion currents were measured on the radial array of collectors as the plate was rotated to various azimuthal angles θ, and the densities were obtained from the currents by using the Bohm formula with $T_e = 3$ eV.
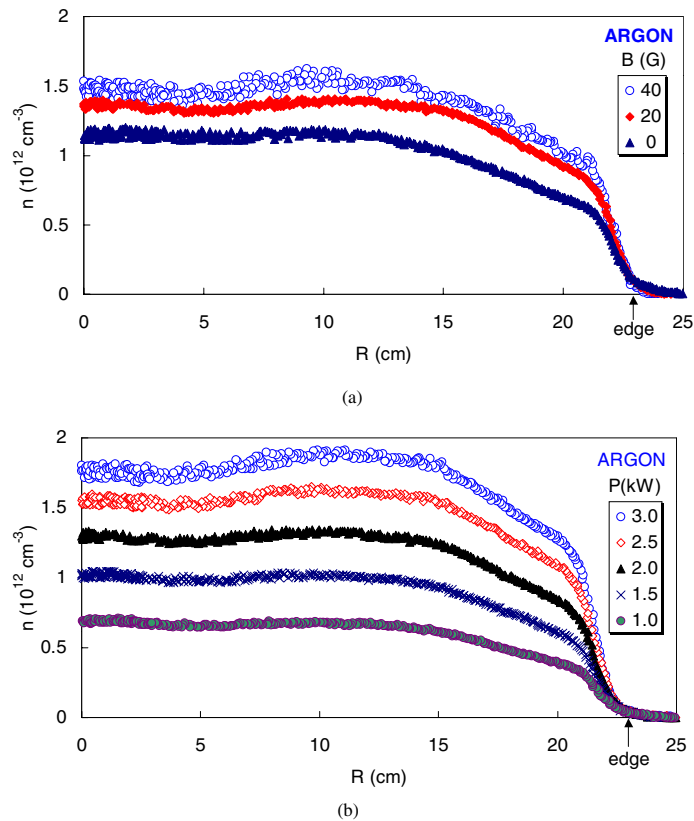
Figure 29. Radial density profiles in argon in a Type 2 source, as functions of (a) B_0 and (b) P_{rf}. 5 mTorr, 20 G, 2 kW, 13.56 MHz, $N = 2$, $z = 7$ cm unless otherwise noted.
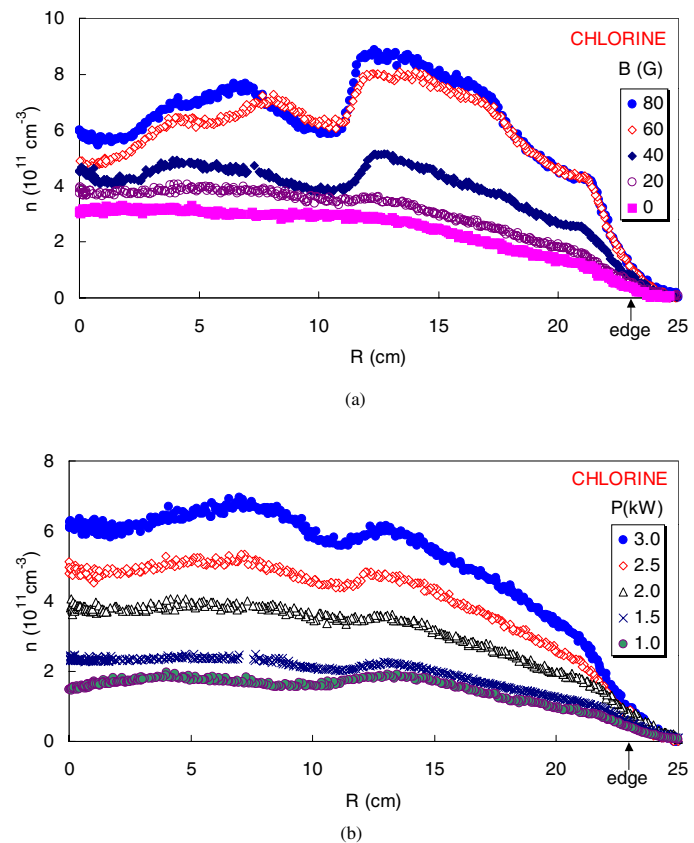
Figure 30. Radial density profiles in chlorine in a Type 2 source, as functions of (a) B_0 and (b) P_{rf}. 3 mTorr, 20 G, 2 kW, 13.56 MHz, $N = 2$, $z = 7$ cm unless otherwise noted.

(a)

(b)
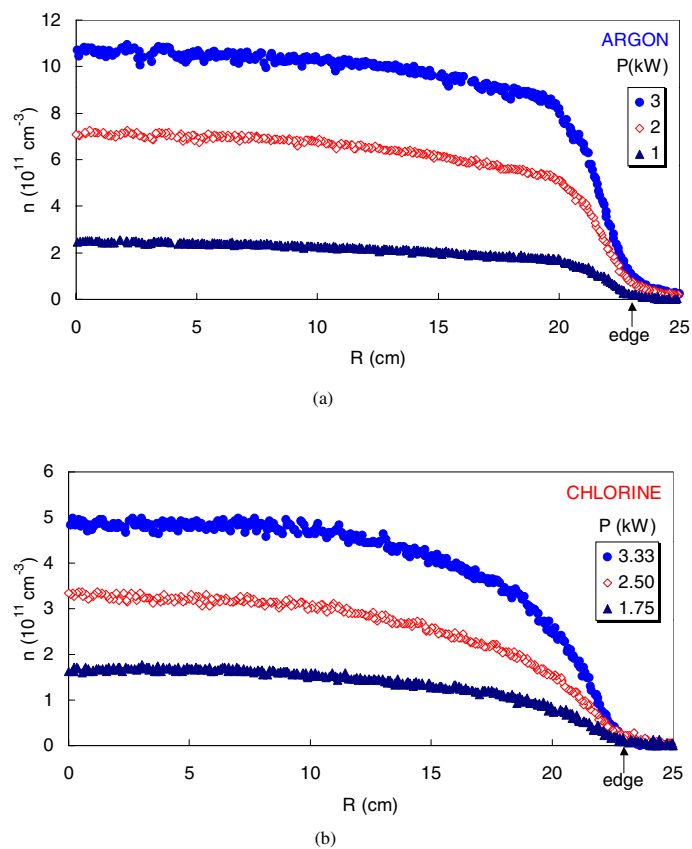
Figure 31. Downstream radial density profiles in (a) 5 mTorr Ar at 20 G and (b) 3 mTorr Cl at 35 G in a Type 2 source. $f = 13.56$ MHz, $N = 2$, $z = 27$ cm.
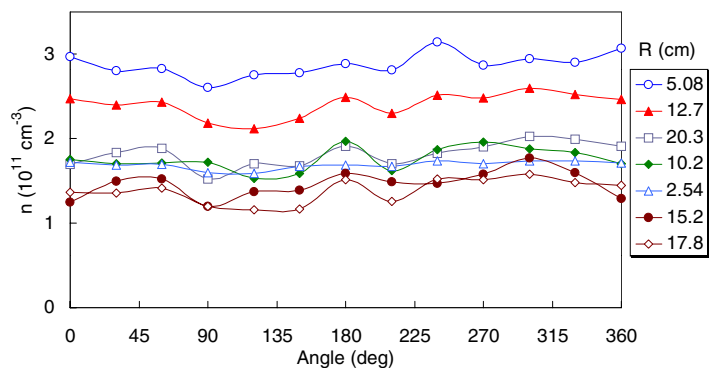
Figure 32. Raw data from the Lazy Susan probe, using a Type 2 array. 3 mTorr Cl, 20 G, 2 kW, 13.56 MHz, $N = 2$, $z = 30$ cm.
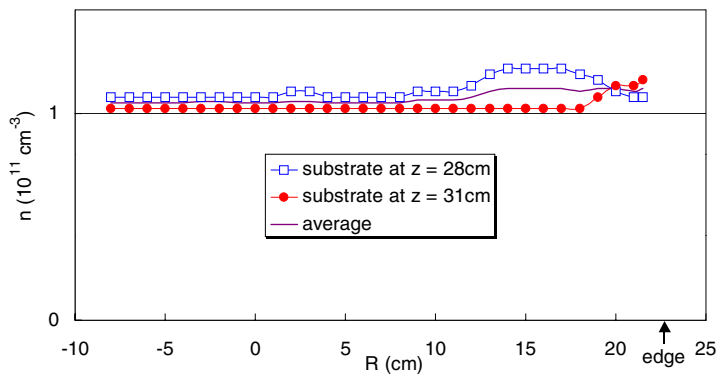
Figure 33. Radial density profile with Langmuir probe at $z = 27.5$ cm, with the Lazy Susan probe defining the plasma boundary ('substrate'), located at $z = 28$ and 31 cm. 2 mTorr Ar, 60 G, 1.4 kW, 13.56 MHz, $N = 4$.
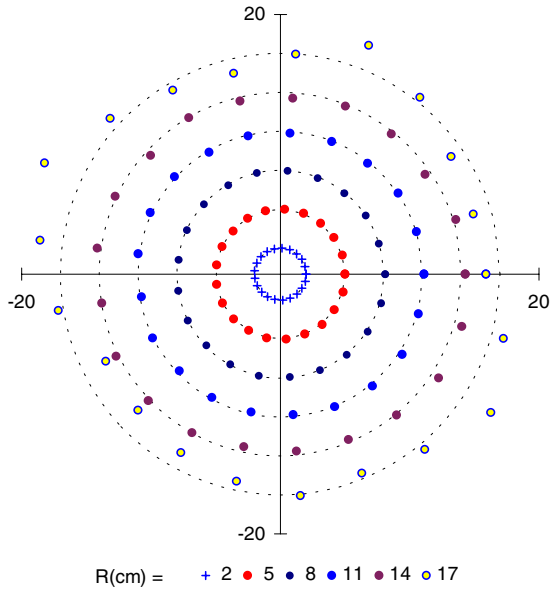
Figure 34. Azimuthal $n(\theta)$ uniformity at various radii in a 40 cm diameter cross section at $z = 30$ cm. The density at each radius is normalized and plotted relative to the dashed circle at that radius. 2 mTorr Ar, 40 G, 1.4 kW, $N = 4$, large chamber.

An example of the raw data is shown in figure 32. It is clear that the collectors have different sensitivities; in order to calibrate them, radial Langmuir probe scans were made

close to the collectors. An example of such a scan is shown in figure 33, where the Lazy Susan probe is moved to axial positions $z = 28$ and 31 cm, acting as the effective plasma boundary ('substrate'). The density 3.5 cm above the collector plate appears to be extremely uniform except near the wall, where the multidipole field of the wall magnets affects the discharge. At 0.5 cm above the plate, there appear to be irregularities due to the collectors themselves. In any case, the deviation from uniformity is much smaller than figure 32 would suggest, and the average of the two curves on figure 33 was used to calibrate the Lazy Susan probe. An example of an azimuthal $n(\theta)$ scan in the large chamber is shown in the polar plot of figure 34. Significant deviation from uniformity can be seen in the outermost curve, but no $m = 6$ azimuthal asymmetry due to the discrete nature of the antenna array is observed. Figure 35 is a polar plot of such a scan in the small chamber, with n plotted radially in absolute units. Deviations from azimuthal uniformity, which manifest themselves as deviations of $n(\theta)$ from a perfectly circular pattern, can be seen for $r > 11$ cm. These data were taken at low n; at higher n, diffusion would improve the uniformity. The density near the wall is shown in figure 36. The periodic structure of the permanent magnet array of the magnetic bucket can be seen, as well as an $m = 1$ asymmetry due to the gas feed near the top of the bucket at $\theta = 225°$ (lower left-hand corner of the polar plots). Again, there is no noticeable $m = 6$ asymmetry due to the six individual outer tubes. A contour plot of absolute $n(r, \theta)$ is shown in figure 37.
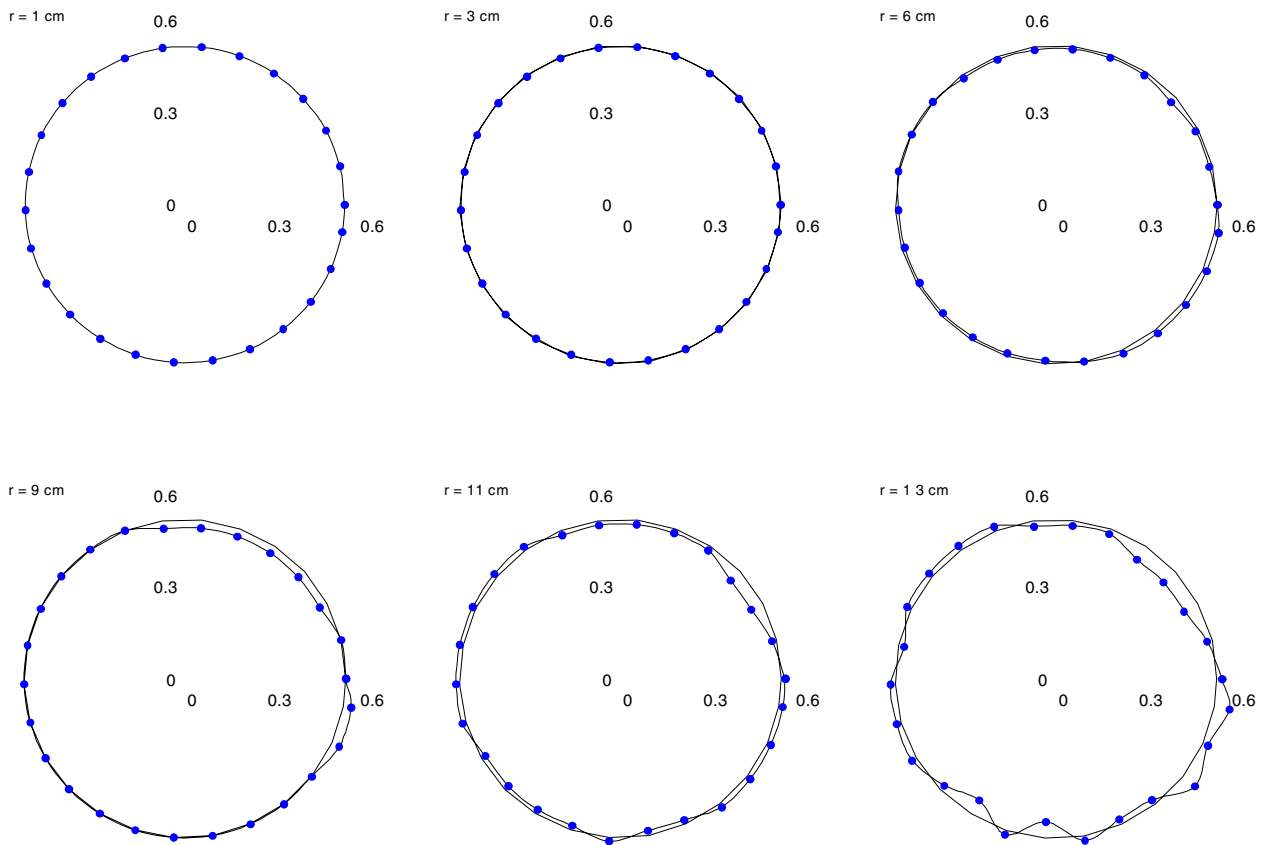
Figure 35. Polar plots of $n(\theta)$ with increasing r in units of 10^{11} cm^{-3}. 20 mTorr Ar, 75 G, 1.3 kW, 13.56 MHz, $z = 20$ cm.
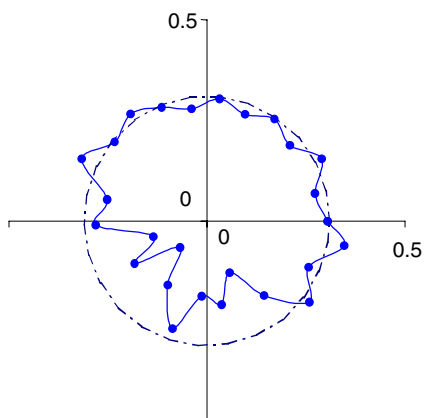
Figure 36. Azimuthal $n(\theta)$ scan at $r = 15$ cm; periodic asymmetry is due to the permanent magnet array on the wall.
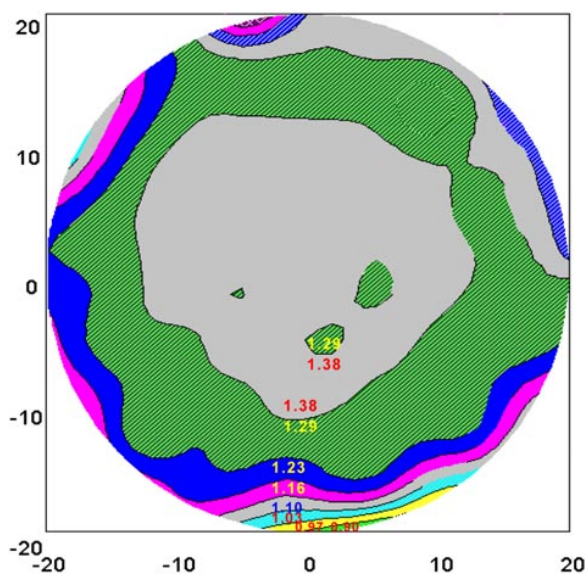
Figure 37. Density contour plot of the data of figure 35. The contours are spaced about 4% apart.
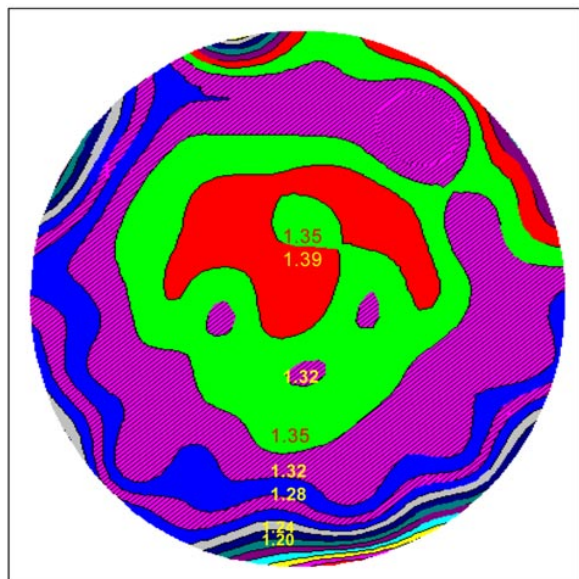
Figure 38. Contour plot of n using two independent rf sources. 15 mTorr Ar, 100 G, 1.6 kW, 27.12 MHz, $N = 2$. The contour interval is 3%.

The uniformity can in principle be improved by using separate power supplies for each tube. To test this, two independent rf sources at 27.12 MHz were used, one driving the central tube and every other outer tube at 920 W, and the other driving the remaining three tubes at 680 W. The density uniformity in figure 37 is thus improved to that of figure 38. Uniformity of $n(r, \theta)$ to within $\pm 3\%$ over most of the area is thus obtained, and there are no indications of an $m = 6$ perturbation in $n(\theta)$ arising from the deployment of the individual tubes.

6. Conclusions

A compact large-area plasma source based on helicon discharges has been designed and tested. Uniform plasmas of density up to 10^{12} cm^{-3} have been produced with multiple sources in a distributed array. Thus, the feasibility of covering large substrates with high-density plasma has been demonstrated in principle. This method can be developed into a plasma processing tool for semiconductor wafers greater than 300 mm in diameter and for flat-panel displays of arbitrary size, as well as for other ultra-large-area plasma processing applications.

Acknowledgments

References

[1] Boswell R W and Chen F F 1997 *IEEE Trans. Plasma Sci.* **25** 1229
[2] Chen F F and Boswell R W 1997 *IEEE Trans. Plasma Sci.* **25** 1245
[3] Arnush D and Chen F F 1998 *Phys. Plasmas* **5** 1239
[4] Shamrai K P, Pavlenko V P and Taranov V eB 1997 *Plasma Phys. Control. Fusion* **39** 505
[5] Mouzouris Y and Scharer J E 1998 *Phys. Plasmas* **5** 4253
[6] Kamenski I V and Borg G G 1998 *Comput. Phys. Commun.* **113** 1
[7] Breizman B and Arefiev A 2000 *Phys. Rev. Lett.* **84** 3863
[8] Chen F F and Blackwell D D 1999 *Phys. Rev. Lett.* **82** 2677
[9] Campbell G A, Pearson D I C and deChambrier A P 1990 *Proc. 33rd Ann. Techn. Conf., Society of Vacuum Coaters*
[10] Chapman B, Benjamin N, van Os C F A, Boswell R W and Perry A J 1991 *Proc. 12th Symp. on Dry Process (Denki-Gakkai, Tokyo, 1991)*
[11] Tynan G R *et al* 1997 *J. Vac. Sci. Technol.* A **15** 2885
[12] Arnush D 2000 *Phys. Plasmas* **7** 3042
[13] Miljak D G and Chen F F 1998 *Plasma Sources Sci. Technol.* **7** 61
[14] Chen F F 1992 *J. Vac. Sci. Technol.* A **10** 1389
[15] Chen F F and Arnush D 1997 *Phys. Plasmas* **4** 3411
[16] Chen F F, Jiang X and Evans J D 2000 *J. Vac. Sci. Technol.* A **18**
[17] Chen F F, Arnush D, Evans J D and Blackwell D D 1998 *Proc. ICPP and 25th EPS Conf. on Controlled. Fusion and Plasma Physics (Praha)* ECA vol 22C, p 2655
[18] Sakawa Y, Koshikawa N and Shoji T 1996 *Appl. Phys. Lett.* **69** 1695
[19] Arnush D 2000 *Phys. Plasmas* **7** 3042
[20] Wu X and Lieberman M A 1998 *Appl. Phys. Lett.* **72** 777
[21] Heinrich F *et al* 1996 *J. Vac. Sci. Technol.* B **14** 2000
[22] Chen F F 1992 Capacitor tuning circuits for inductive loads *UCLA Report* PPG-1401